Epitaxial Growth of MgxCa1−xO on GaN by Atomic Layer Deposition

Epitaxial Growth of $Mg_xCa_{1-x}O$ on GaN by Atomic Layer Deposition

Xiabing Lou[†], Hong Zhou[‡], Sang Bok Kim[†], Sami Alghamdi[‡], Xian Gong[†], Jun Feng[†], Xinwei Wang[†#], Peide D. Ye[‡], Roy G. Gordon[†]

[†]Department of Chemistry and Chemical Biology, Harvard University, Cambridge, Massachusetts 02138, United States

‡School of Electrical and Computer Engineering and Birck Nanotechnology Center, Purdue University, West Lafayette, Indiana 47906, United States

Corresponding Author: Roy G. Gordon, Email: gordon@chemistry.harvard.edu

Present Address:

[#] School of Advanced Materials, Shenzhen Graduate School, Peking University, Shenzhen 518055, China

Abstract: We demonstrate for the first time that a single-crystalline epitaxial $Mg_{1-x}Ca_xO$ film can be deposited on gallium nitride (GaN) by atomic layer deposition (ALD). By adjusting the ratio between the amounts of Mg and Ca in the film, a lattice matched $Mg_xCa_{1-x}O$/GaN(0001) interface can be achieved with low interfacial defect density. High resolution X-ray diffraction (XRD) shows that the lattice parameter of this ternary oxide nearly obeys Vegard's Law. An atomically sharp interface from cross-sectional transmission electron microscopy (TEM) confirmed the high quality of the epitaxy. High temperature capacitance-voltage characterization showed that the

film with composition $Mg_{0.25}Ca_{0.75}O$ has the lowest interfacial defect density. With this optimal oxide composition, a $Mg_{0.25}Ca_{0.75}O$/AlGaN/GaN metal-oxide-semiconductor high-electron-mobility (MOS-HEMT) device was fabricated. An ultra-high on/off ratio of 10^{12} and a near ideal SS of 62mV/dec was achieved with this device.

KEYWORDS: Epitaxy, dielectric, GaN, MOS-HEMT, magnesium calcium oxide

The wide implementation of solar energy and fast development of electrical vehicles both require more efficient power electronic devices working under high voltage (>600V), high temperature (>100 ^{o}C) and high frequency conditions.[1] Currently, Si-based power devices could not meet these demands due to the small band gap (1.1 eV) and low breakdown field of Si.[2] GaN could replace Si for future power applications because of its higher band gap (3.4eV) and higher breakdown field. However, unlike Si, the interface trap density between GaN and its native oxide (Ga_2O_3) is huge, which prevents high efficiency modulation of GaN devices. Many alternative dielectrics, such as HfO_2,[3] Al_2O_3,[4] SiO_2,[5] Sc_2O_3,[6] etc, have been employed as dielectrics on GaN in various studies. However, GaN devices with a low defect interface and high quality dielectric have not been achieved with any material.

Recently, our group demonstrated that ALD can grow lanthanum oxide epitaxially on

gallium arsenide (GaAs) (111)A surfaces, and that the density of interfacial defects is remarkably low.[7] Although the (0001) surface of GaN wurtzite structure has an atomic structure similar to the (111)A surface of GaAs, it is more challenging to apply the same strategy to GaN due to the lack of any lattice matched oxide. We have also reported ALD-Sc_2O_3 growth on AlGaN/GaN based HEMT devices.[6] Due to the large lattice mismatch between Sc_2O_3 and the substrate (~9%), epitaxial growth could not be achieved. MgO and CaO, both have relatively high dielectric constants (MgO 9.8, CaO 11.8) and large band gaps (both 7~8 eV), and thus might be suitable gate oxides for GaN. Moreover, the GaN lattice size lies between those of the MgO and CaO lattices (mismatch -6.5% for MgO and +6.5% for CaO). Therefore, by tuning the composition of $Mg_xCa_{1-x}O$, a lattice match with GaN substrates can be achieved. Hellman et al.[8] demonstrated that epitaxial $Mg_{1-x}Ca_xO$ can be grown by molecular beam epitaxy (MBE) on MgO substrates. Later, Paisley et al.[9] and Ren et al.[10] reported that epitaxial $Mg_{0.5}Ca_{0.5}O$ can be grown on GaN with the same method. Measurements on HEMTs with MBE-fabricated MgCaO insulators showed improved gate-lag.[11] However, MBE is not applicable to large substrates needed for cost-effective industrial processing. Thus a more scalable and lower cost method to deposit epitaxial $Mg_xCa_{1-x}O$ is highly desirable.

In this work, we demonstrate that atomic layer deposition (ALD) can form $Mg_xCa_{1-x}O$ epitaxially on GaN(0001). Cross sectional transmission electron microscopy (TEM)

determined the relationship of this heteroepitaxy to be (111)×[011]$Mg_xCa_{1-x}O$//GaN(0001)×[11-20]. High-resolution X-ray diffraction (HRXRD) and electron diffraction (ED) showed that the lattice constants of $Mg_xCa_{1-x}O$ with different compositions are close to the predictions of Vegard's Law. Capacitance-voltage (C-V) measurements were employed to study the interfacial defects and $Mg_{0.25}Ca_{0.75}O$ showed the lowest density of defects. Additionally, an ultra-high on/off ratio of 10^{12} and a near-ideal subthreshold swing of 62mV/dec were achieved with $Mg_{0.25}Ca_{0.75}O$ as a gate oxide of GaN MOS-HEMT. This is the first demonstration of epitaxial $Mg_xCa_{1-x}O$ in a GaN/AlGaN/GaN MOS-HEMT device. The results show that the $Mg_xCa_{1-x}O$ dielectric is promising for applications in high-frequency and power electronics.

ALD of $Mg_xCa_{1-x}O$ was carried out in a home-built tubular reactor[12]. Bis(*N*,*N*'-diisopropylacetamidinato)calcium(II) dimer[13], bis(*N*,*N*'-di-*sec*-butylacetamidinato)magnesium[14] and H_2O were used as calcium, magnesium and oxygen sources, respectively. Structural formulas for the Mg and Ca precursors are shown in **Fig. 1**. Three different precursor dosing ratios, namely Mg:Ca=1:1, Mg:Ca=1:2 and Mg:Ca=1:3, were employed. The compositions of the resulting films were determined by Rutherford Backscattering Spectroscopy (RBS) to be $Mg_{0.72}Ca_{0.28}O$, $Mg_{0.51}Ca_{0.49}O$ and $Mg_{0.25}Ca_{0.75}O$, respectively. The detailed growth conditions are summarized in supporting information. The depositions below a

substrate temperature of 290 ^{o}C were not well crystalized while carbon impurity can be detected at above 330 ^{o}C. Therefore, an optimal growth temperature is determined to be 310 ^{o}C. The film growth rates with different dosing ratios and the corresponding compositions are summarized in **Table 1**. For all three compositions, the growth rates are slightly smaller than a linear combination of the MgO and CaO growth rates, and the Mg contents are higher than their corresponding dosing ratio in the 1:1 and 1:2 cases. This indicates that the MgO cycle might have a hindering effect on the reaction of the CaO deposition cycle. Although MgO and CaO are nearly immiscible at equilibrium below 2000 ^{o}C,[15] this solid mixture is kinetically stable up to about 600 ^{o}C.[16]

One powerful method to examine the epitaxial film quality is cross-sectional TEM imaging. **Figure 2** summarizes the cross-section TEM images of three different $Mg_xCa_{1-x}O$/GaN samples. Since GaN and $Mg_xCa_{1-x}O$ have different crystal structures, their lattice patterns in TEM are different. The GaN region shows a distinctive three atomic line periodicity pattern in the vertical direction while $Mg_xCa_{1-x}O$ does not have this feature. All three samples show sharp interfaces without any interfacial layer. The nearly perfect single crystal lattices in **Fig. 2 a** and **b** confirmed the high quality of epitaxy of $Mg_{0.25}Ca_{0.75}O$ and $Mg_{0.51}Ca_{0.49}O$ on GaN. On the other hand, the grain boundaries in **Fig. 2 c** indicate that a highly textured $Mg_{0.72}Ca_{0.28}O$ film is formed on GaN. The well-defined film spots in the diffraction pattern (**Fig. S2**) also confirmed

the high quality of epitaxial $Mg_{0.25}Ca_{0.75}O$ and $Mg_{0.51}Ca_{0.49}O$ films while the $Mg_{0.72}Ca_{0.28}O$ film has some textured features. Moreover, from the diffraction pattern, the zone axis of the GaN substrate in these TEM images is [11-20], while the film zone axis can be determined as [011]. Therefore, the epitaxial relation between the film and substrate is (111)×[0-11] $Mg_xCa_{1-x}O$ //GaN(0001)×[11-20].

In order to study the lattice mismatch between $Mg_xCa_{1-x}O$ film and GaN substrate, coupled 2θ-ω HRXRD scans were employed. Both GaN(0004) and $Mg_xCa_{1-x}O$(222) peaks are seen in all three samples (**Fig. 3 a**). The absence of MgO and CaO peaks indicates that phase separation into the two binaries has not occurred. The $Mg_xCa_{1-x}O$(222) peak shifts to lower 2θ position as the Ca content increases. Both measured lattice constants and the calculated lattice constants based on Vegard's Law are plotted in **Fig. 3 b**. Assuming a fully relaxed hetero-epitaxial relation at the interface and considering the epitaxial relationship between the film and the substrate, the out-of-plane lattice mismatch can be defined as: $(a_{MgCaO(222)}-a_{GaN(0004)})/ a_{GaN(0004)}$.[7] The mismatch is -1.2% for $Mg_{0.72}Ca_{0.28}O$, +2.4% $Mg_{0.51}Ca_{0.49}O$ and +3.1% for $Mg_{0.25}Ca_{0.75}O$. Similar lattice mismatch values obtained from in-plane FFT analysis of TEM cross-sectional images also confirmed the relaxed interface. (**Fig. S8**) Despite the larger lattice mismatch, $Mg_{0.51}Ca_{0.49}O$ and $Mg_{0.25}Ca_{0.75}O$ show nearly perfect epitaxy while $Mg_{0.72}Ca_{0.28}O$, with a smaller mismatch, exhibits a textured structure. Such results indicate that there might be factors other than mismatch affecting the

epitaxial quality.

Although MgO and CaO are immiscible with each other below 2000 ^{o}C[15], previous reports[9,17] have shown that $Mg_xCa_{1-x}O$ can be grown by MBE at lower temperature without phase separation. In order to examine the microscopic crystallinity and phase composition of the $Mg_xCa_{1-x}O$ films deposited by this ALD method, transmission electron microscopy (TEM) was employed. As shown in supporting information, the ring diffraction pattern in **Fig. S1 (b)** clearly indicates that film is polycrystalline on SiN_x. The relative positions between different diffraction rings in the electron diffraction pattern are in accord with the FCC standard pattern. This indicates that the $Mg_xCa_{1-x}O$ shares the same rock salt structure with MgO and CaO. Additionally, the values of the lattice spacings lie in between the corresponding spacings in MgO and CaO, showing that the $Mg_xCa_{1-x}O$ film is a uniform alloy of the two components without phase separation.

In summary of the above structural characterizations, $Mg_xCa_{1-x}O$ films deposited by ALD were proved to be epitaxial on GaN by both TEM and XRD. Cross sectional TEM revealed near perfect epitaxy of $Mg_{0.51}Ca_{0.49}O$ and $Mg_{0.25}Ca_{0.75}O$ on GaN. However, although a smaller lattice mismatch was found in $Mg_{0.72}Ca_{0.28}O$/GaN, the epitaxy was not as perfect as for the other two compositions. Therefore lattice mismatch might not be the only parameter affecting the quality of epitaxy.

$Mg_xCa_{1-x}O$/GaN MOS-capacitor devices were fabricated to examine the electrical performance by capacitance-voltage and conductance-voltage measurements. Since GaN has a wide band gap of 3.4eV, a room temperature CV does not effectively probe defects near the middle of the bandgap. Therefore, the MOS-capacitors were measured at 150 ^oC as well as at room temperature. Due to the hydroscopic nature of $Mg_xCa_{1-x}O$, 5 nm of Al_2O_3 were deposited as a capping layer to keep moisture away from the $Mg_xCa_{1-x}O$ layer. An amorphous Al_2O_3/GaN MOS was also prepared for comparison. A "top-to-top" capacitor structure was used to measure the capacitance due to the insulating sapphire substrate under the GaN (**Fig. S3**). In this measurement, the positive probe is placed in contact with the gate electrode while the negative probe is in contact with the large area of GaN covered by aluminum metal. Since the gate has a serial connection with the large area, the measured capacitance is given by $1/C_m = 1/C_g + 1/C_l$, where C_m is the capacitance measured by the LCR meter, C_g is the capacitance of the gate and C_l is the capacitance of the larger area. Since $C_\ell >> C_g$, the measured capacitance is dominated by the gate: $C_m \approx C_g$.

The measured room temperature and high temperature CV curves from three $Mg_xCa_{1-x}O$ /GaN samples as well as an Al_2O_3/GaN sample are summarized in **Fig. 4**. In room temperature studies (**Fig. 4 a**, **b** and **c**), very small (<6%) frequency dispersion can be seen in the depletion region for all three $Mg_xCa_{1-x}O$ samples, while

there is a 20% dispersion in the same region in the Al_2O_3/GaN sample (**Fig. 4 d**). In the absence of interface traps, dispersion should not occur. Therefore the reduced dispersion in the three $Mg_xCa_{1-x}O$ samples compared to the Al_2O_3 sample qualitatively indicates that the epitaxial film did reduce the number of interfacial traps. Due to the low interfacial trap density, a numerical value for D_{it} could not be extracted from the room temperature CV measurements. During the CV measurement, the Fermi level is moved deeper in the band gap at a higher temperature; thus defect information can be obtained over a wider range of energies within the band gap.[18] In the CV data taken at 150 ^oC (**Fig. 4 e, f, g and h**), the frequency dispersion remained relatively small (<6%) for all three $Mg_xCa_{1-x}O$ samples while the dispersion in Al_2O_3/GaN is as large as 100%. The smaller frequency dispersion at high temperature indicates that the $Mg_xCa_{1-x}O$ film effectively reduced the interfacial trap density near the midgap region compared to Al_2O_3. In order to measure the D_{it} values quantitatively, the conductance method was employed since the Terman method is considered less sensitive[19] and the Gray-Brown method is not applicable to III-V semiconductors.[20] The detailed measurement procedure and conductance data are summarized in the supporting information(**Fig. S5**).[18] The measured values of D_{it} are summarized in **Fig. 4 i**. Two of the samples with epitaxial films show the lowest D_{it} values, while the textured sample has about one order of magnitude higher interfacial trap density. Although the lattice mismatch of the $Mg_{0.25}Ca_{0.75}O$ sample is slightly larger than that of the other two $Mg_xCa_{1-x}O$ samples, the measured D_{it} level is the lowest (~5×10^{12} $eV^{-1}cm^{-2}$). One possible explanation is that during the early ALD

cycles, the Ca growth rate is smaller than that of the Mg. Thus the Ca content near the interface is lower than in the bulk $Mg_xCa_{1-x}O$ film. Another possible explanation is that a trace amount of $Mg(OH)_2$ may also cause interfacial traps, while adding more Ca content may help reduce the number of hydroxyl groups and therefore reduce the D_{it} level. The dielectric constant of the $Mg_{0.25}Ca_{0.75}O$ film derived from the CV measurement is 10, which is close to the permittivities of MgO and CaO.

The ultimate goal of developing this material is implementing $Mg_xCa_{1-x}O$ into GaN MOS-HEMT devices with unprecedented oxide/semiconductor interface quality. A schematic cross section of such a device is shown in **Fig. 5 a**. The fabrication process is summarized in supporting information. The $Mg_{0.25}Ca_{0.75}O$ film was used as the gate dielectric in this study due to its lower D_{it}. The gate oxide stack is Al_2O_3(5nm)/$Mg_{0.25}Ca_{0.75}O$(10nm)/GaN. Well-behaved I_d-V_{ds} and linear-scale I_d-V_{gs} curves (**Fig. 5 b** and **d**) show the good control capability of the GaN MOS-HEMT. **Fig. 5** c shows the transfer characteristics in a log-scale plot at V_{ds}=1 V and 5 V, respectively. This device possesses an ultra-high on/off ratio 10^{12} due to the high quality interface. Thus the channel can be shut off completely. This value is two orders of magnitude higher than those HEMT devices with Al_2O_3 passivation.[21] In addition to the ultra-high on/off ratio, the GaN MOS-HEMT also possesses a near ideal subthreshold swing (SS) of 62 mV/dec, further confirming the high quality interface between GaN and the $Mg_{0.25}Ca_{0.75}O$ layer.[22] The successful implementation

of the $Mg_{0.25}Ca_{0.75}O$ into a GaN MOS-HEMT shows that it's promising for use in GaN MOS technology.

Epitaxial $Mg_xCa_{1-x}O$ films have been successfully grown on GaN [0001] surfaces using ALD for the first time. The crystallographic relationship of this hetero-epitaxy has been studied in detail. Moreover, the potential of applying this unprecedentedly high-quality dielectric film has been evaluated with C-V characterization, revealing that the density of defects is affected by not only the lattice mismatch but also by the composition of the film. $Mg_{0.25}Ca_{0.75}O$ is found to provide the interface with the fewest traps and the MOS-HEMT made from it exhibits an ultra-high on/off ratio of 10^{12} and a near ideal SS of 62 mV/dec. Thus we believe this epitaxial $Mg_xCa_{1-x}O$ film can provide improved high-frequency and high-power electronics in the future.

Dosing ratio Mg:Ca	Average growth rate (nm/cycle)	Composition	Lattice constant (nm)	Vagard's Law prediction (nm)
CaO	0.075	CaO	0.1389	0.1389
1:3	0.05	$Mg_{0.25}Ca_{0.75}O$	0.134	0.1345
1:2	0.05	$Mg_{0.51}Ca_{0.49}O$	0.133	0.1299
1:1	0.06	$Mg_{0.72}Ca_{0.28}O$	0.128	0.1262
MgO	0.05	MgO	0.1213	0.1213

Table 1.Summary of ALD growth rates, compositions and lattice constants of different $Mg_xCa_{1-x}O$ films. The composition was measured by Rutherford back scattering (RBS). Lattice constants of $Mg_xCa_{1-x}O$ (222) were measured by HRXRD. MgO and CaO (222) lattice constants were from Crystallography Open Database.

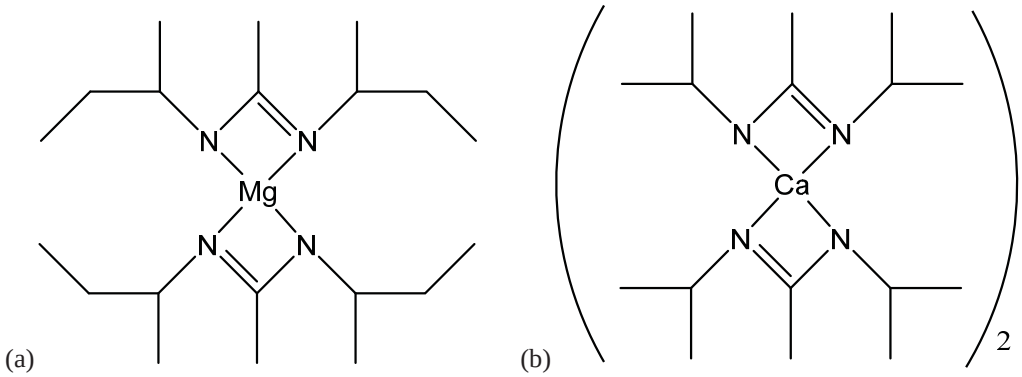

Figure 1. Structures of the metal precursors. (a) bis(*N*,*N'*-di-*sec*-butylacetamidinato)magnesium; (b) bis(*N*,*N'*-diisopropylacetamidinato)calcium(II) dimer.

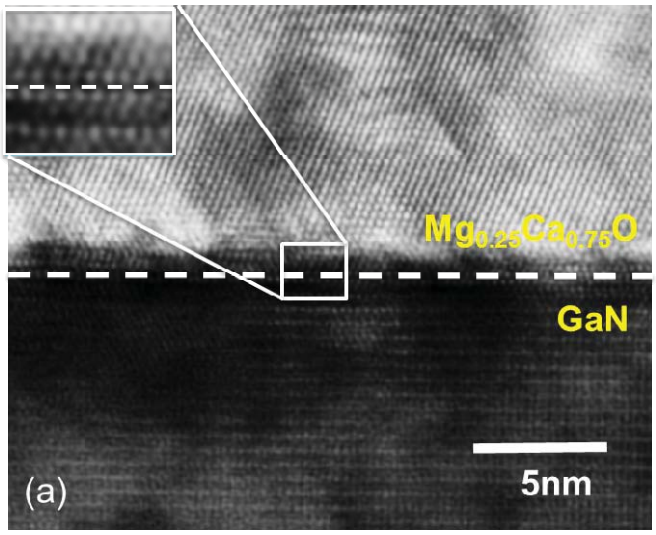
$Mg_{0.25}Ca_{0.75}O$
GaN
5nm
(a)

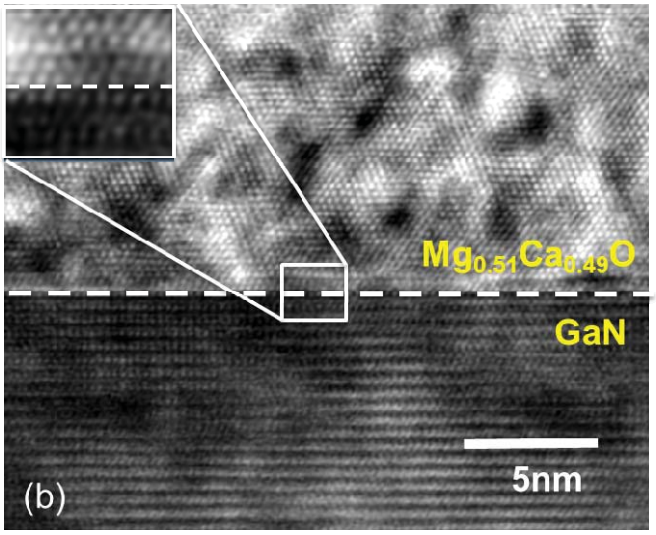
$Mg_{0.51}Ca_{0.49}O$
GaN
5nm
(b)

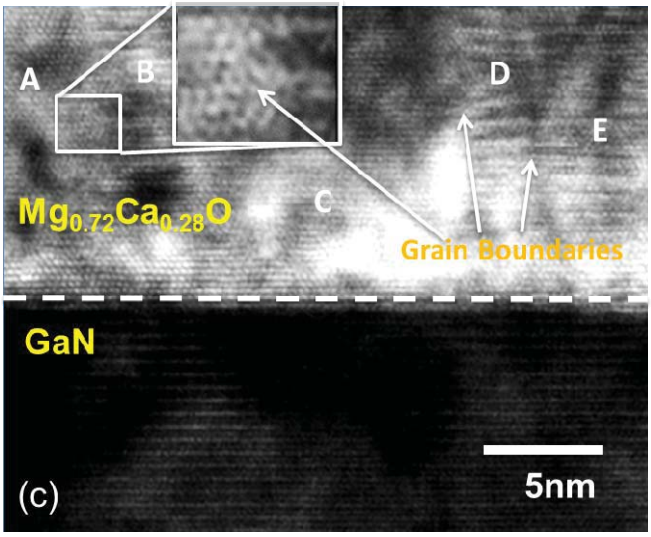
A
B
C
D
E
$Mg_{0.72}Ca_{0.28}O$
Grain Boundaries
GaN
5nm
(c)

Figure 2. Cross-sectional TEM of $Mg_xCa_{1-x}O$ films grown on GaN(0001) surface. (a) $Mg_{0.25}Ca_{0.75}O$/GaN; (b) $Mg_{0.51}Ca_{0.49}O$/GaN; (c) $Mg_{0.72}Ca_{0.28}O$/GaN, grain boundaries can be found between each region labeled with letters. The enlarged grain boundary between region A and B shows both darkness contrast as well as pattern difference. Region B is showing a three line repeating pattern, which indicates two different orientation grains are overlapping together. Similar pattern can also be found in regions D and E.

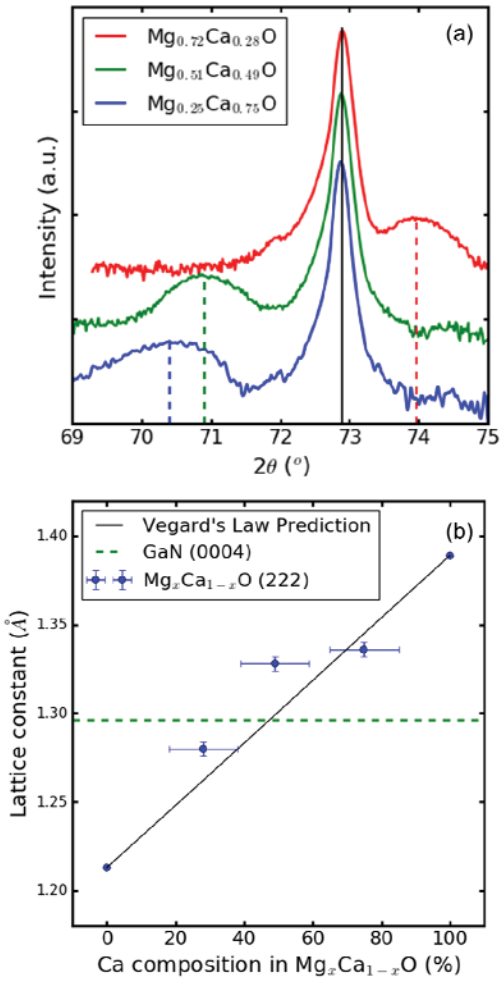

Figure 3. Lattice constant study by HRXRD. (a) HRXRD study of $Mg_xCa_{1-x}O$/GaN film. The black vertical line is the peak position of GaN(0004) diffraction. The dashed lines represent the peak positions of the $Mg_xCa_{1-x}O$ (222) diffractions; (b) Vegard's Law predicted lattice constant vs XRD measured poly-crystalline $Mg_xCa_{1-x}O$ (222) lattice constants. The green dashed line is the lattice constant that matches the GaN(0004) lattice.

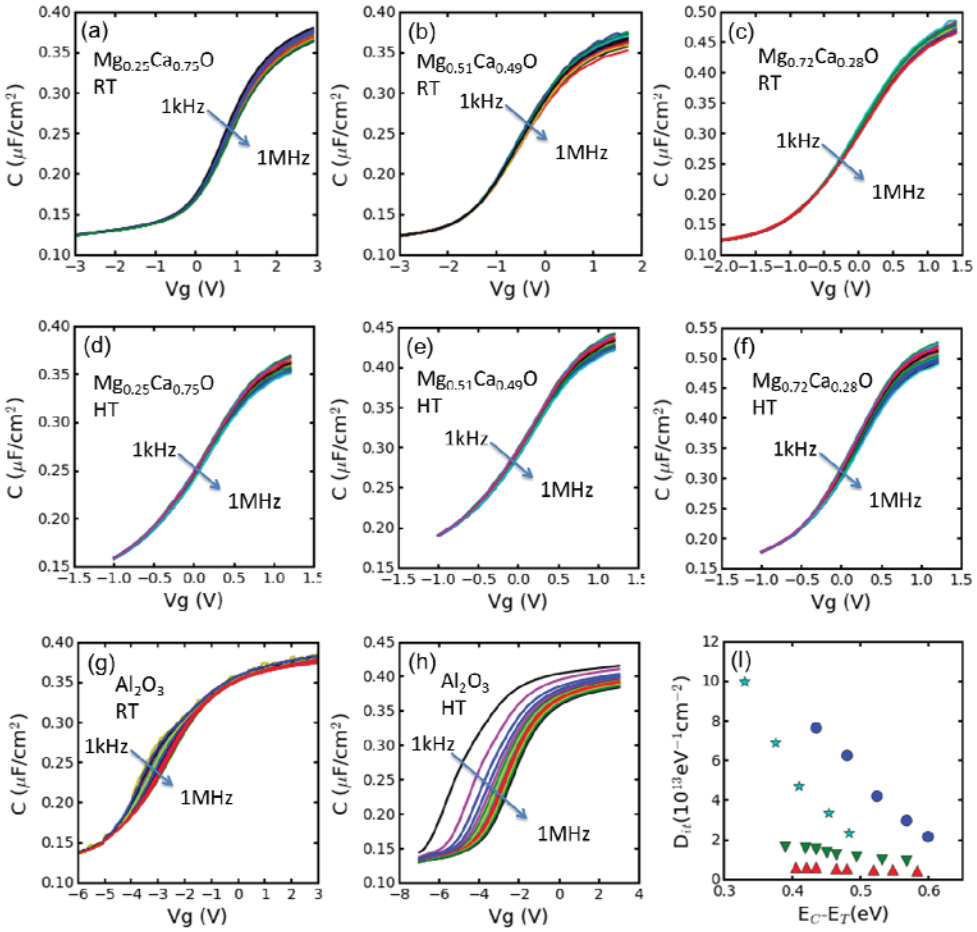

Figure 4. C-V measurements for $Mg_xCa_{1-x}O$/GaN and Al_2O_3/GaN samples. The frequency ranges of all samples are from 1kHz to 1MHz. (a) 20°C Al_2O_3(5nm)/$Mg_{0.25}Ca_{0.75}O$(15nm)/GaN; (b) 20°C Al_2O_3(5nm)/$Mg_{0.51}Ca_{0.49}O$(15nm)/GaN; (c) 20°C Al_2O_3(5nm)/$Mg_{0.72}Ca_{0.28}O$(15nm)/GaN; (d) 150°C Al_2O_3(5nm)/$Mg_{0.25}Ca_{0.75}O$(15nm)/GaN. (e) 150°C Al_2O_3(5nm)/$Mg_{0.51}Ca_{0.49}O$(15nm)/GaN; (f) 150°C Al_2O_3(5nm)/$Mg_{0.72}Ca_{0.28}O$(15nm)/GaN; (g)20°C Al_2O_3(20nm)/GaN for comparison; (h) Al_2O_3(20nm)/ GaN; (i) D_{it} summary of four samples determined by the conductance method: Al_2O_3(20nm)/ GaN (light blue star ★), Al_2O_3(5nm)/$Mg_{0.72}Ca_{0.28}O$(15nm)/GaN (blue circles ●), Al_2O_3(5nm)/$Mg_{0.51}Ca_{0.49}O$(15nm)/GaN (green down triangle ▼) and Al_2O_3(5nm)/$Mg_{0.25}Ca_{0.75}O$(15nm)/GaN(red up triangles▲)

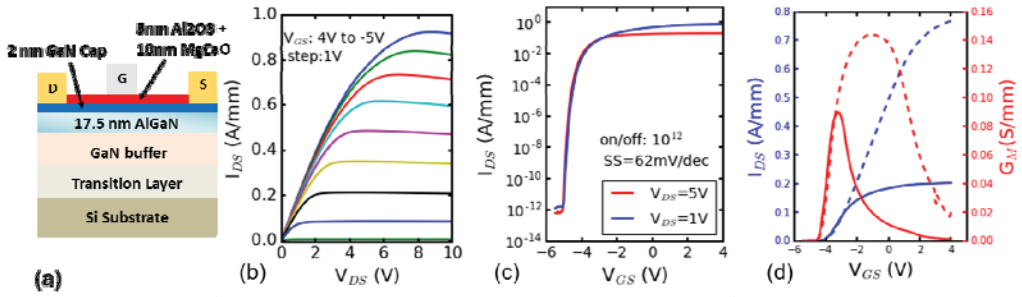

Figure 5. MOS-HEMT device performance characterization. a) Schematic of the $Mg_xCa_{1-x}O$ MOS-HEMT device; b) Transfer characteristics of the $Mg_{0.25}Ca_{0.75}O$/GaN/AlGaN/GaN MOS-HEMT device; c) I-V characteristics comparison between two different source drain voltage; d) Conductivity and current vs gate voltage study. Solid lines represent V_{DS} = 5 V, dashed lines represent V_{DS} = 1 V.

Supporting Information

Methods, TEM diffraction patterns of $Mg_xCa_{1-x}O$/GaN, MOS-HEMT and MOS-capacitor fabrication, AC conductance method to extract D_{it}.

Acknowledgements

The work at Harvard University is supported by the Center for the Next Generation of Materials by Design, an Energy Frontier Research Center funded by the U.S. DOE, Office of Science. The work at Purdue University is supported in part by AFOSR (FA9550-12-1-0180) and in part by Award N000141512833 from ONR. Some of the work was performed at Harvard University's Center for Nanoscale Systems (CNS), a member of the National Nanotechnology Infra-Structure Network (NNIN) and at Harvard's X-ray laboratory. We would like to thank Kelson Chabak from AFRL for providing the high-quality AlGaN/GaN on Si wafers for this research.

References

(1) Hensel, A.; Wilhelm, C.; Kranzer, D. *IEEE Int. Power Electron. Motion Control Conf.* **2012**, DS3d.4-1-DS3d.4-5.

(2) Ikeda, N.; Li, J.; Kato, S.; Masuda, M.; Yoshida, S. *Furukawa Rev.* **2006**, No. 29, 1–6.

(3) Tang, Z. J.; Li, R.; Yin, J. *J. Mater. Sci. Mater. Electron.* **2014**, *25* (1), 152–156.

(4) Kang, H.-S.; Reddy, M. S. P.; Kim, D.-S.; Kim, K.-W.; Ha, J.-B.; Lee, Y. S.; Choi, H.-C.; Lee, J.-H. *J. Phys. D. Appl. Phys.* **2013**, *46* (15), 155101.

(5) Huang, W.; Khan, T.; Chow, T. P. *J. Electron. Mater.* **2006**, *35* (4), 726–732.

(6) Wang, X.; Saadat, O. I.; Xi, B.; Lou, X.; Molnar, R. J.; Palacios, T.; Gordon, R. G.; Palacios, T.; Gordon, R. G. *Appl. Phys. Lett.* **2012**, *101* (23), 232109.

(7) Wang, X.; Dong, L.; Zhang, J.; Liu, Y.; Ye, P. D.; Gordon, R. G. *Nano Lett.* **2013**, *13* (111), 594–599.

(8) Hellman, E. S.; Hartford, E. H. *Appl. Phys. Lett.* **1994**, *64* (11), 1341–1343.

(9) Paisley, E. A.; Gaddy, B. E.; Lebeau, J. M.; Shelton, C. T.; Biegalski, M. D.; Christen, H. M.; Losego, M. D.; Mita, S.; Collazo, R.; Sitar, Z.; Irving, D. L.; Maria, J.-P. P. *J. Appl. Phys.* **2014**, *115* (6), 64101.

(10) Chen, J.-J.; Hlad, M.; Gerger, A. P.; Gila, B. P.; Ren, F.; Abernathy, C. R.; Pearton, S. J. *J. Electron. Mater.* **2007**, *36* (4), 368–372.

(11) Gila, B. P.; Hlad, M.; Onstine, A. H.; Frazier, R.; Thaler, G. T.; Herrero, A.; Lambers, E.; Abernathy, C. R.; Pearton, S. J.; Anderson, T.; Jang, S.; Ren, F.; Moser, N.; Fitch, R. C.; Freund, M. *Appl. Phys. Lett.* **2005**, *87* (16), 163503.

(12) Wang, X. Applications of Vapor Deposition in Microelectronics and Dye-Sensitized Solar Cells, Harvard University, 2013.

(13) Kim, S. B.; Yang, C.; Powers, T.; Davis, L. M.; Lou, X.; Gordon, R. G. *Angew. Chem. Int. Ed.* **2016**, *55*, 10228–10233.

(14) de Rouffignac, P.; Sullivan, N.; Beaulieu, D.; Park, J.-S.; Hock, A.; Gordon, R. G. In *Proceedings of the AVS Atomic Layer Deposition Conference*; 2009.

(15) Doman, R. C.; Barr, J. B.; Mcnally, R. N.; Alper, A. M. *J. Am. Ceram. Soc.* **1963**, *46*, 313–316.

(16) Li, H. D.; Zhang, X. N.; Zhang, Z.; Mei, Z. X.; Du, X. L.; Xue, Q. K. *J. Appl. Phys.* **2007**, *101* (10), 2005–2008.

(17) Gila, B. P.; Thaler, G. T.; Onstine, A. H.; Hlad, M.; Gerger, A.; Herrero, A.; Allums, K. K.;

Stodilka, D.; Jang, S.; Kang, B.; Anderson, T.; Abernathy, C. R.; Ren, F.; Pearton, S. J. *Solid. State. Electron.* **2006**, *50* (6), 1016–1023.

(18) Matocha, K.; Gutmann, R. J.; Chow, T. P. *IEEE Trans. Electron Devices* **2003**, *50* (5), 1200–1204.

(19) E. H. Nicollian andA. Goetzberger. *Bell Syst. Tech. J.* **1967**, *46* (6), 1055–1033.

(20) Brown, D. M.; Gray, P. V. *J. Electrochem. Soc.* **1966**, *155* (7), 760–766.

(21) Yang, S.; Tang, Z.; Wong, K. Y.; Lin, Y. S.; Liu, C.; Lu, Y.; Huang, S.; Chen, K. J. *IEEE Electron Device Lett.* **2013**, *34* (12), 1497–1499.

(22) Bin Lu, B.; Min Sun, M.; Palacios, T. *IEEE Electron Device Lett.* **2013**, *34* (3), 369–371.

Table of Content Figure

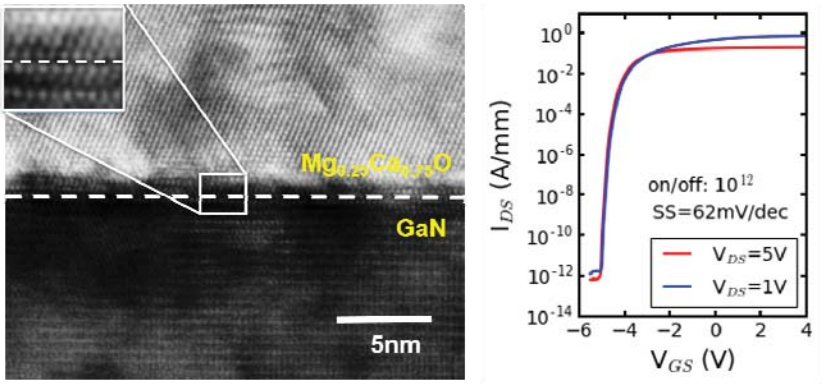

Supporting Information

Epitaxial Growth of $Mg_xCa_{1-x}O$ on GaN by Atomic Layer Deposition

Xiabing Lou[†], Hong Zhou[‡], Sang Bok Kim[†], Sami Alghamdi[‡], Xian Gong[†], Jun Feng[†], Xinwei Wang[†#], Peide D. Ye[‡], Roy G. Gordon[†]

[†]Department of Chemistry and Chemical Biology, Harvard University, Cambridge, Massachusetts 02138, United States

‡School of Electrical and Computer Engineering and Birck Nanotechnology Center, Purdue University, West Lafayette, Indiana 47906, United States

Correspondence to: gordon@chemistry.harvard.edu

Present Address:

[#] School of Advanced Materials, Shenzhen Graduate School, Peking University, Shenzhen 518055, China

XRR/XRD

$Mg_xCa_{1-x}O$ grown on thermal oxide (300nm SiO_2/Si) wafers was characterized by XRD and XRR for lattice spacing and thickness respectively. Each thermal oxide wafer was cleaned of organic contamination by exposure to UV light in air (UV-ozone treatment) for 5 min before being loaded into the deposition chamber. Both XRR and XRD characterization was performed with a Bruker D8 Discover system.

Deposition conditions for ALD

The magnesium and calcium precursors were kept in sealed bubblers at 110 ^{o}C and 140 ^{o}C respectively in two separate ovens, and were delivered into the reaction chamber with controlled volumes of N_2 carrier gas. The deposition was performed at a substrate temperature of 310 ^{o}C. The dosing sequence was $[(Ca\text{-}H_2O)_y\text{-}(Mg\text{-}H_2O)_x]_n$. Each metal precursor dose was followed by a water dose. The composition was adjusted by varying the dosing ratio between the Mg and Ca cycles. The GaN substrates were treated with UV-Ozone for 5min then followed with 20% ammonium hydroxide soaking for 20min prior to ALD deposition. The water contact angle on newly received GaN substrate was 70^{o}. This hydrophobic surface was due to the adsorbed organic compounds. After removal of organic contamination by UV-Ozone treatment, the contact angle decreased down to 18^{o} since the surface was turned into Ga_2O_3. The contact angle of GaN surface further decreased to 9^{o} after ammonium hydroxide treatment. This was because the ammonium hydroxide could effectively remove the Ga_2O_3 and expose the clean and highly hydrophilic GaN surface for deposition.[1] Such surface is highly favorable for a Frank–van der Merwe (layer-by-layer) growth in ALD.

FIB/TEM

Transmission electron microscopy (TEM) images were taken with a JEOL-2100 TEM at the Harvard Center for Nanoscale Systems (CNS). The TEM cross-section sample preparation was done with a FEI Helios 660 focused ion beam (FIB) system.

Top view TEM of $Mg_{0.25}Ca_{0.75}O/Si_3N_4$ membrane and its diffraction pattern in **Fig. S1** confirmed that no phase separation into MgO and CaO occurred.

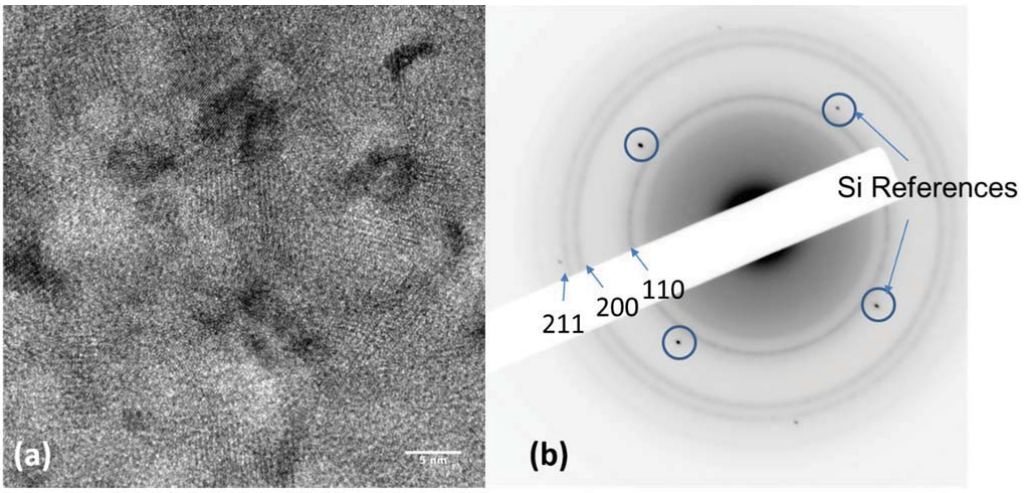

Figure S1. (a) Top view of $Mg_{0.25}Ca_{0.75}O/Si_3N_4$ membrane. (b) TEM diffraction pattern of the area in (a).

In the cross section TEM diffraction patterns (**Fig. S2**), as Mg content increases, the MgCaO (-200) and (-111) diffraction spots shift farther from the center of the pattern. This trend is accord with the HRXRD results shown in **Fig 2.** The MgCaO (111) diffraction spots are overlapped with the GaN (0002) spot.

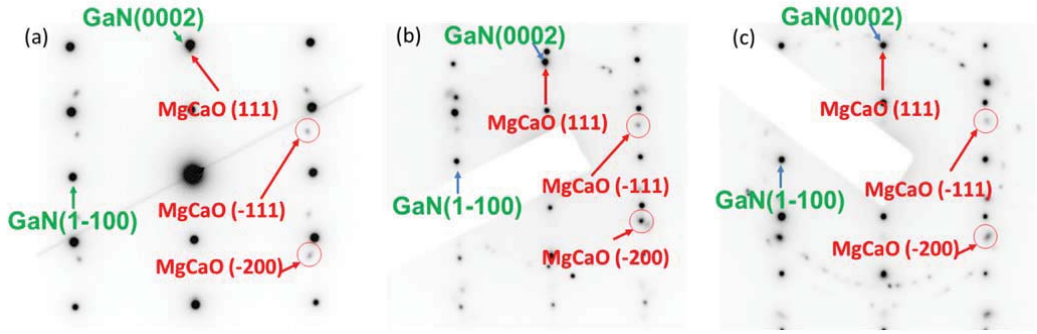

Figure S2. TEM diffraction pattern of cross sectional $Mg_xCa_{1-x}O$/GaN interface sample. The zone axis is GaN [-1 -1 2 0]. (a) $Mg_{0.25}Ca_{0.72}O$/GaN; (b) $Mg_{0.51}Ca_{0.49}O$/GaN; (c) $Mg_{0.72}Ca_{0.28}O$/GaN.

RBS

Rutherford Backscattering Spectroscopy (RBS) was done at the Department of Physics and Astronomy, Rutgers University.

MOS-capacitor

Epi-layers GaN (5μm thick) grown on sapphire substrates were purchased from MTI with resistivity of 0.02 Ω • cm. The GaN wafers were treated with UV-ozone for organic removal and then soaked for 20 min in 20% aqueous ammonium hydroxide to remove native oxides. After pretreatment the samples were patterned into circular capacitors by photo lithography. 300nm Al metal was then deposited onto the dielectric and the remaining photoresist with thermal evaporation. After lift-off overnight, the "top-to-top" capacitor structure was formed as shown in **Fig. S3**

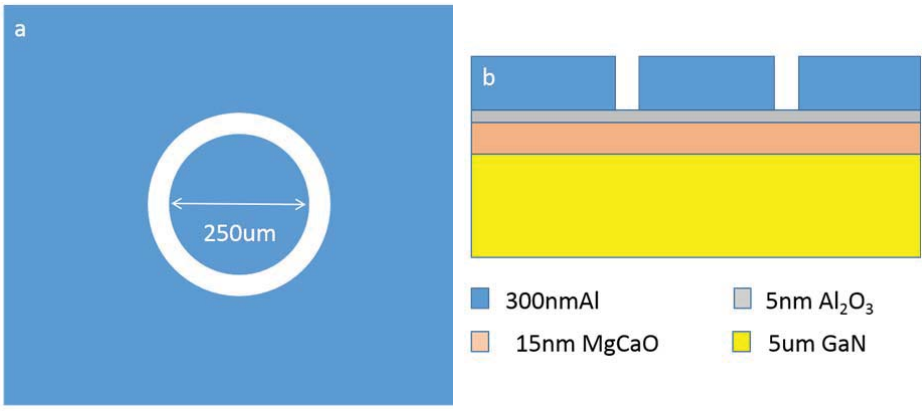

Figure S3. MOS-capacitor for CV measurement. (a) Top view of the MOS-capacitor. (b) Side view of the MOS-capacitor.

MOS-HEMT

The AlGaN/GaN MOS-HEMT structure was grown on a Si (111) substrate, consisting of, a 5-nm Al_2O_3 capping layer, a 10-nm $Mg_{0.25}Ca_{0.75}O$ epitaxial oxide, a 2-nm GaN capping layer, a 17-nm $Al_{0.26}Ga_{0.74}N$ barrier, a 1-nm AlN spacer, a GaN channel, and a 800 nm GaN buffer. Device fabrication started with mesa isolation by Cl_2/BCl_3 etching to a depth of 80 nm. Then, Ohmic contacts were formed by depositing Ti/Al/Ni/Au (20/100/40/50 nm) followed by 775 °C rapid thermal anneal in N_2 atmosphere. The sheet resistance (R_{SH}) and contact resistance (R_C) were determined to be 480 Ω/□ and 0.3 Ω·mm through transfer length method (TLM). Then gate oxides were deposited by ALD. The gate metal is formed by deposition of Ni/Au (30/50 nm) with lift-off process. Electrical measurements were performed with a Keysight E4980A LCR meter.

MOS-HEMT measurement conditions

I_D-V_{DS}: The V_{DS} is swept from 0 to 10 V and the V_{GS} is stepped from 5 V to -5 V with -0.5 V as the step.

I_D-V_{GS}: The V_{GS} is swept from 4 V to -5.5 V with -0.05 V as a step at V_{DS}=1 V and 5 V.

AC conductance method to extract D_{it}

The AC conductance method is one of the most sensitive methods to determine D_{it}. The equivalent circuits of the MOS capacitor are as following in **Fig S4**:

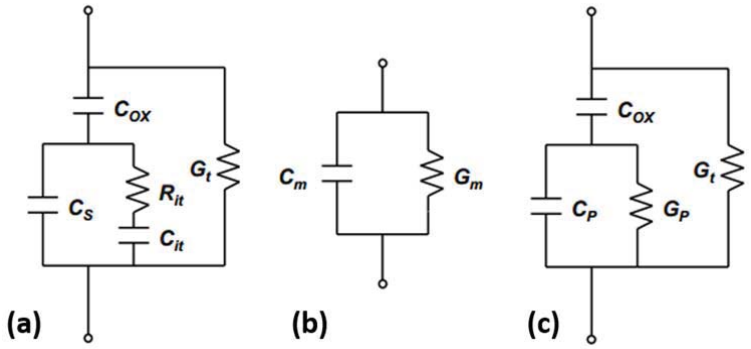

Figure S4. Equivalent circuits of MOS capacitor; (a) an equivalent circuit model of the

MOS capacitor, (b) the measured circuit, (c) the simplified circuit of (a).

The extracted D_{it} can be expressed by the following equation:

$$D_{it} = \frac{2.5}{q}\left(\frac{G_p}{\omega}\right)_{max}$$

where G_p/ω is

$$\frac{G_p}{\omega} = \frac{\omega(G_m - G_t)C_{ox}^2}{G_m^2 + \omega^2(C_{ox} - C_m)^2}$$

C_{ox}, C_m, G_m and G_t are oxide capacitance, measured capacitance, measured conductance, and measured oxide tunnel conductance, respectively.

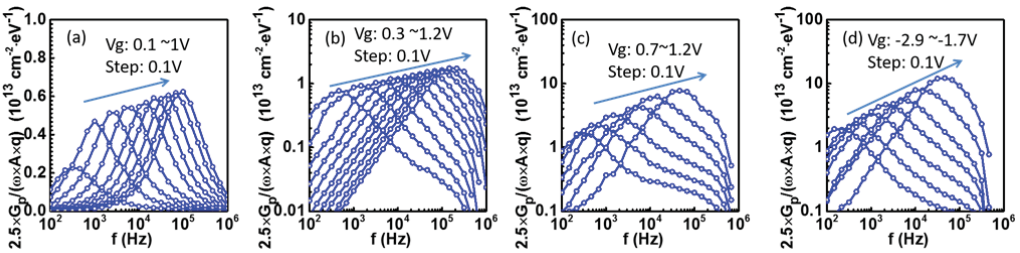

Figure S5. G_p/ω vs. frequency at 150 ^{o}C. (a) Al_2O_3(5nm)/$Mg_{0.25}Ca_{0.75}O$(15nm)/GaN. (b) Al_2O_3(5nm)/$Mg_{0.51}Ca_{0.49}O$(15nm)/GaN. (c) Al_2O_3(5nm)/$Mg_{0.72}Ca_{0.28}O$(15nm)/GaN. (d) Al_2O_3(20nm)/ GaN;

The trap energy level within the bandgap can be expressed as:

$$\Delta E = \mathrm{kT} \times \ln\left(\frac{\sigma V_T N}{2\pi \mathrm{f}}\right)$$

where k, T, σ, V_T, N, and f are Boltzmann constant, temperature, trap capture cross section, thermal velocity, conduction band density, and conductance peak corresponding frequency, respectively.

XPS

X-ray photoelectron spectroscopy (XPS) was taken by a Thermo Scientific K-alpha system. In **Fig S6**, the absence of Ga and N signals from substrate in $Mg_{0.25}Ca_{0.75}O$/GaN indicates that the surface of GaN is fully covered by MgCaO film. Since the penetration depth of XPS and the film thickness in this case were both about 10 nm, any missing areas of the film would result in detectable substrate signals. Therefore, the absence of substrate signal indicates that the film is uniformly covering the GaN surface.

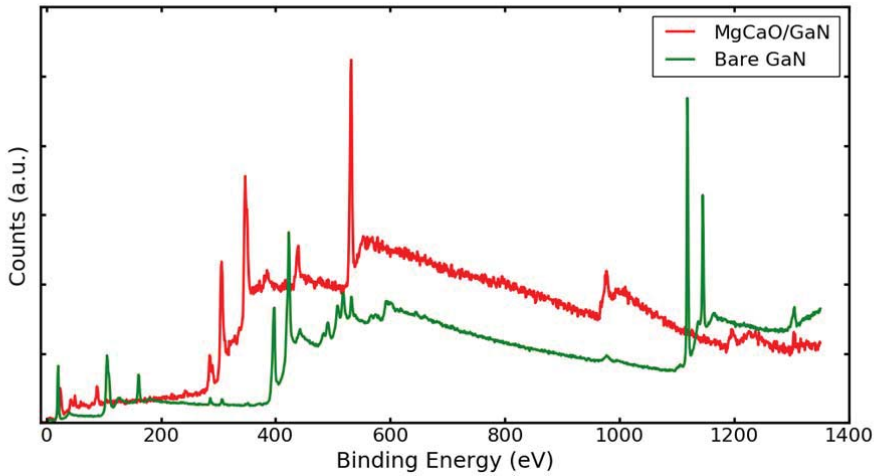

Figure S6. XPS spectrum of bare GaN (green) and $Mg_{0.25}Ca_{0.75}O$(10nm)/GaN (red).

AFM

The AFM study is done with an Asylum MFP-3D AFM System. The similar RMS values obtained from before and after the deposition indicate that the film has uniform thickness.

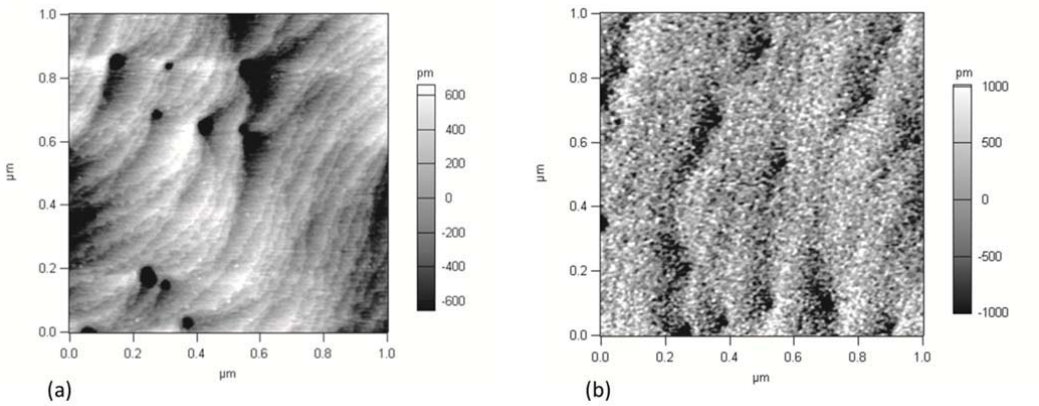

Figure S7. (a) GaN surface, RMS = 0.37 nm; (b) $Mg_{0.25}Ca_{0.75}O$(10nm)/GaN surface, RMS = 0.47 nm

FFT analysis of crosssectional TEM images.

Fast Fourier Transform (FFT) analysis is employed to study the in-plane lattice mismatch. By measuring the lateral distance of corresponding spots in the FFT images with pixel as unit, the in-plane lattice mismatch can be calculated with $(L_{sub}-L_{film})/L_{film}$. The error range of in-plane mismatch from FFT is about ±1% due to the limited image resolution. The results show that the in-plane mismatch is in good agreement with the out-of-plane mismatch.

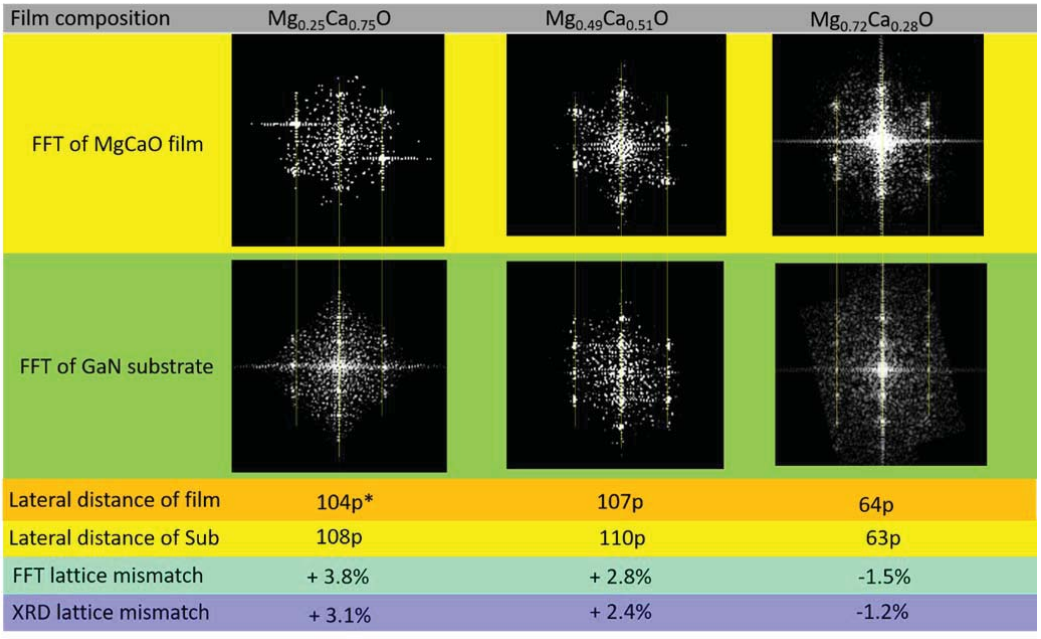

Figure S8. Fast Fourier Transform analysis of MgCaO/GaN crosssection TEM images. The original images are from **Fig 2**. * "p" stands for pixels in the image.

Reference

(1) King, S. W.; Barnak, J. P.; Bremser, M. D.; Tracy, K. M.; Ronning, C.; Davis, R. F.; Nemanich, R. J. *J. Appl. Phys.* **1998**, *84* (9), 5248–5260.